SPECT/CT for Dosimetry

2

Stephan Walrand

2.1 Introduction

Likely, most nuclear clinicians will naturally acknowledge that SPECT/CT is the best tool beside PET/CT to get an accurate individual dosimetry in internal radiotherapy. But is it really needed? Often, internal radiotherapies are performed without any real individual dosimetry assessment. So why should we use the state-of-the-art SPECT/CT system?

This practice is linked with two wrong beliefs commonly spread in the nuclear medicine community: increasing the tumour's absorbed dose a little bit can just improve a little bit the patient outcome and the efficacy of external photon beam radiotherapy improved because the irradiation devices improved, so our only option is also to improve our tumour tracers.

The first belief comes from the way we are used to assess the efficacy of internal radiotherapies, i.e. by measuring the change in tumour size or in metabolism a few months after the therapy. And indeed, in this case, increasing a little bit the absorbed dose just increases a little bit the response, as early tissue (organ or tumour) toxicity is a smooth function of the absorbed dose [1–5]: killing a fraction of the tissue cells reduces the tissue metabolism by a similar fraction.

However, late tissue toxicity owns an absorbed dose threshold [6–8]: above a critical fraction of cells killed, the tissue will not be able to recover and will "die". Decay, production of free radicals by ionisation, and hits of the radicals to the DNA are all random processes. The recovering capacity of a tissue depends on its state. As a result, the normal tissue complication probability (NTCP) and the tumour control probability (TCP) are not step functions but are quite steeply S-shape functions, i.e. going from 0 to 1 within a few Gy. In addition, the dosimetry of critical organs is highly patient dependent [1]. It is thus of paramount importance to give the

S. Walrand, PhD
Nuclear medicine, Université Catholique de Louvain, Brussels, Belgium
e-mail: stephan.walrand@uclouvain.be

H. Ahmadzadehfar, H.-J. Biersack (eds.), *Clinical Applications of SPECT-CT*,
DOI 10.1007/978-3-642-35283-6_2, © Springer-Verlag Berlin Heidelberg 2014

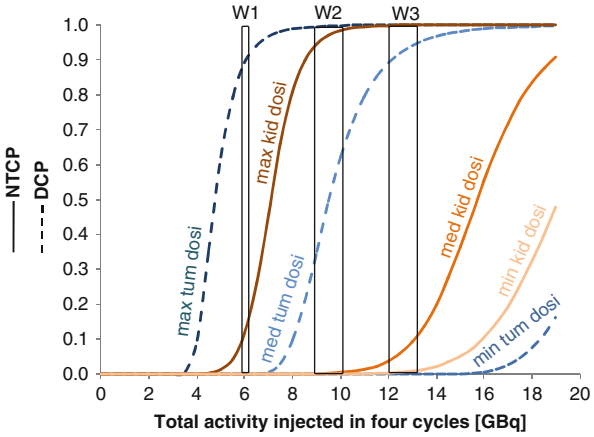

Fig. 2.1 Illustration of the therapeutic windows (TW) concept applied to ^{90}Y-DOTATOC PRRT. The disease control probability (DCP) and kidney NTCP were computed for their respective minimum, median and maximum dosimetry measured by ^{86}Y-DOTATOC PET in the phase 1 clinical study using amino acid infusion [1, 9]. The curves were computed for a disease owning five tumours, and the tissue radiation tolerance parameters were extracted from [6, 10]. For a patient owning both the median tumour and median kidney dosimetry, W3 is a good TW choice giving a probability of 90 % to be curative and of 10 % to get a late renal failure. If his tumour dosimetry is the maximal one observed, then W2 is a better choice avoiding any risk of late renal failure. A patient with the maximal kidney dosimetry observed can be cured only if he also owns the maximal tumour dosimetry observed (*W1*)

maximal activity to the patient that is still safe for him. Indeed, for some patients the resulting increase in the tumour-absorbed dose, even small, could be sufficient to shift from a cancer relapse to a controlled disease. In external beam radiotherapy (EBRT) this feature is called the therapeutic window. Figure 2.1 illustrates this concept applied to ^{90}Y-DOTATOC used in peptide receptor radiotherapy (PRRT). Even, if dosimetry assessments are not accurate enough to ensure being in narrow therapeutic windows, the maximal chance for the patient outcome is to be as close as possible to his individual therapeutic window.

During the last decades, the efficacy of EBRT and the sophistication of the devices used have increased together. From these points of view, the recent CyberKnife system is really impressive [11]. In reality, there is no real innovation regarding the CyberKnife hardware (the knife part): it is the combination of a linear accelerator and of a standard industrial 6-axis robot used in car manufacturing, both existing for three decades. So why this system appeared only recently? The major benefit of the CyberKnife is to allow decreasing the absorbed dose to the critical tissues by increasing the number of different beam paths crossing the patient body to target the tumour. This (the cyber part) required motion tracking and an accurate individual treatment planning that uses state-of-the-art multimodality imaging [12–14] including elaborated Monte Carlo simulations of the absorbed dose spreading along the beam paths. This feasibility results from the continuous development of such treatment planning assessment in EBRT during the last decades [15].

Internal radiotherapy had the good fortune to begin with two pathologies owning a large therapeutic window: the radio-synovectomy and the thyroid cancer ^{131}I radio-ablation. These two therapies were used with success by simply injecting a standard activity. Sometimes, an early success durably formats the behaviours, and despite a lot of efforts spent during two decades, no such ideal radio-compound was found for the other cancers. For the patient's benefit and also for the long-term future of nuclear medicine, we have to push the available internal radiotherapies to their optimal efficiency by performing an individual treatment planning at the same quality level as that routinely performed in EBRT. Let it be emphasised that a dosimetry method displaying a good dose–toxicity correlation on a patient's sample is not sufficient: As the goal is to inject to the patient the maximal activity that he can safely receive, the dosimetry has to be accurate on a patient per patient basis.

2.2 SPECT Versus Planar

There are four effects which definitely disqualify the use of planar-based dosimetry in most of internal radiotherapies: (1) γ-rays attenuation-scatter, (2) tissues overlapping, (3) multi-compartment organ and (4) heterogeneous organ uptake.

1. There is no way to accurately correct gamma rays attenuation in planar acquisition: use of conjugated planar views, even jointly with a planar transmission scan, is a crude approximation. This method is only valid for an infinitely thin organ without any other activity overlapping. Use of a point scatter kernel to correct for the organ's cross-contamination is hampered by the lack of information about the activity depth distribution. This cross-contamination is very cumbersome regarding that biological half-life of the organs is different and that the critical organs can be located close to tissue owning higher activity, such as liver, spleen, tumour and bowels close to the kidneys in PRRT.
2. The critical organs can partially or fully be overlapped by higher taking up tissues. Often, this problem is casually considered, and several papers proposed patient dosimetry assessment based on planar views using correction method for the overlapping tissues. But to our knowledge only one [16] presented a validation on phantoms, which should be done for all proposed methods. However, these phantoms were simple: no full overlap, identical effective half-life for the different tissues, and no appearing and disappearing activities (bowel in PRRT). Let it be emphasised that such overlap correction methods have to accurately work for the worst patient case to whom it is not ethically defendable to tell that we cannot do an accurate treatment planning, because we chose to not use the best tool.

   Sandström et al. [17] compared the absorbed dose assessed from conjugate planar views and SPECT/CT in 24 patients imaged 1, 24, 96 and 168 h post-^{177}Lu-DOTATATE therapy. Both modalities were corrected for attenuation: a ^{57}Co transmission scan was performed with the planar modality for this purpose. The planar view to SPECT total kidney absorbed dose ratio ranged from 0.8 to

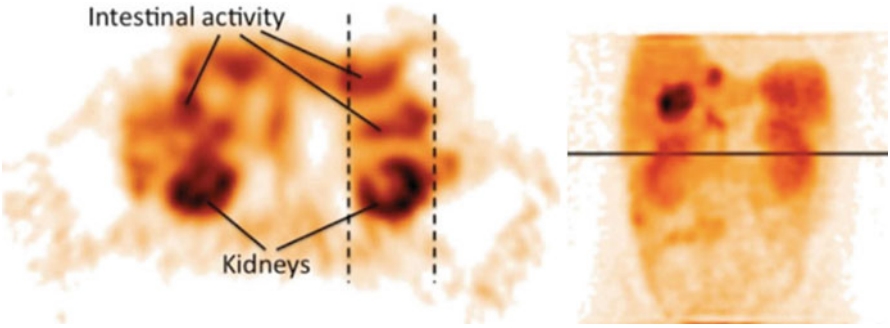

Fig. 2.2 Two images illustrating an imaging situation that results in an overestimated absorbed dose to the kidneys. The activity uptake in the contents of the intestine that overlaps the kidney in the planar image (as indicated by *dashed lines*) contributes to the absorbed dose, which is not the case in the single-photon emission computed tomography image. Note that the overlapping activity is difficult to detect in the planar images (Reprinted from Garkavij et al. [18] with permission of John Wiley and Sons)

5.4: 6 patients out of 24 had a relative deviation higher than 40 %. This clearly disqualifies planar imaging in PRRT pre-therapy planning. Garkavij et al. [18] observed the same problem, in 16 patients also treated with ^{177}Lu-DOTATATE, although with a lower maximal planar view to SPECT total kidney absorbed dose ratio: 1.8. The reason explaining this huge discrepancy between planar and SPECT-based dosimetry, in both studies, originated from significant radioactivity overlap as illustrated in Fig. 2.2. In an older ^{90}Y-DOTATOC study, Valkema et al. reported that organs overlapping preventing accurate planar dosimetry assessment occurred in 6 out of 43 patients [19].

3. Some critical organs own several compartments displaying different uptakes, biological washouts and radiosensitivities. For example, in PRRT, the renal cortex and medulla represent about 70 and 30 % of the kidney activity, respectively [20]. The critical tissue, i.e. the glomerular, is located into the cortex. The medulla to cortex S-factor is about one fourth of that from the cortex to the cortex [21]. The volume, uptake and biological washout of these compartments are also patient dependent [1, 22]. These three points require separately assessing the number of decays occurring in the medulla and in the renal cortex, which cannot be done in planar view.
4. Even if the organ has a homogeneous radiosensitivity, i.e. the spatial variations of the radiosensitivity are smaller than the ionising particle range, such as the liver in ^{90}Y-radioembolisation, assessing the intra-organ absorbed dose distribution is still needed. Indeed, studies have shown that the NTCP does not depend only on the mean organ absorbed dose but also on its distribution [23, 24]. NTCP can be calculated using the equivalent uniform dose (EUD) formalism that accounts for the absorbed dose distribution [10]. For homogeneous density organs, the EUD can be computed based on a fast convolution of the SPECT image by a dose deposition kernel, preferably deconvolved by the SPECT system spatial resolution [25].

Lastly, the argument, which is still sometimes advanced nowadays [16], that planar views have to be used because SPECT is too much time consuming is not relevant. Irradiating a patient from the inside is a medical act as serious as irradiating him from the outside and should be done in the same sophisticated way.

2.3 SPECT/CT Versus SPECT

Hybrid SPECT/CT system allows a better co-registration accuracy of the two modalities than that obtain by trying to acquire the patient with exactly the same geometry in two different systems or than to use delicate nonrigid fusion. This favourably impacts the activity quantification. Regarding dosimetry assessment, this also helps to link the activity observed to the tissue owning it.

Activity quantification requires the knowledge of the patient attenuation map. SPECT systems equipped with a gamma ray transmission source are rare. The attenuation map can be derived from the CT Hounsfield values using appropriate rescaling [26]. The issue regarding the additional irradiation received by the patient from the CT performed at the different SPECT time points needed to assess the pharmacokinetics is purely philosophical regarding the four higher order of magnitude of the absorbed dose received during the therapy.

Recent literature review showed that SPECT/CT performed better in absolute quantification than conventional SPECT system [27]. On acquisitions of a torso phantom, Shcherbinin et al. [28] reported errors between 3 and 5 % for the isotopes ^{99m}Tc, ^{123}I, ^{131}I and ^{111}In. The phantom contained two sources centrally and peripherally placed with no surrounding activity. For ^{99m}Tc in a cardiac torso phantom, Vandervoort et al. [29] reported an error of 8 % in simulation and within 4 % for the acquisition. Both studies included attenuation, scatter and collimator PSF in the iterative reconstruction.

Willowson et al. [30] evaluated SPECT/CT quantification for ^{99m}Tc in phantoms and in patients. The acquisitions were first corrected for scattering using a transmission-dependent scatter correction (TDSC) method developed on site and afterwards reconstructed with a commercial OSEM software. The scatter-corrected data, the associated reconstructed data and the co-registered attenuation map were then passed to an iterative Chang attenuation correction algorithm using the CT-derived attenuation correction map. Last, a dead-time correction was performed. In the torso phantom, the relative deviation of the total liver-specific activity assessment was 2 %. Clinical evaluation in 12 lung ventilation/perfusion studies after injection of calibrated ^{99m}Tc-MAA activity gave a relative deviation ranging from −7.4 to 3.7 % (mean absolute relative deviation of 2.6 %).

Beauregard et al. [31] evaluated a commercially available SPECT/CT system in quantitative ^{177}Lu imaging using the manufacturer's iterative reconstruction algorithm that included CT-based attenuation correction, scatter correction using a triple-energy acquisition window and collimator PSF. In addition, they added a camera sensitivity calibration function of the count rate in order to correct for the dead time. They performed seven acquisitions of a 20 cm diameter phantom with

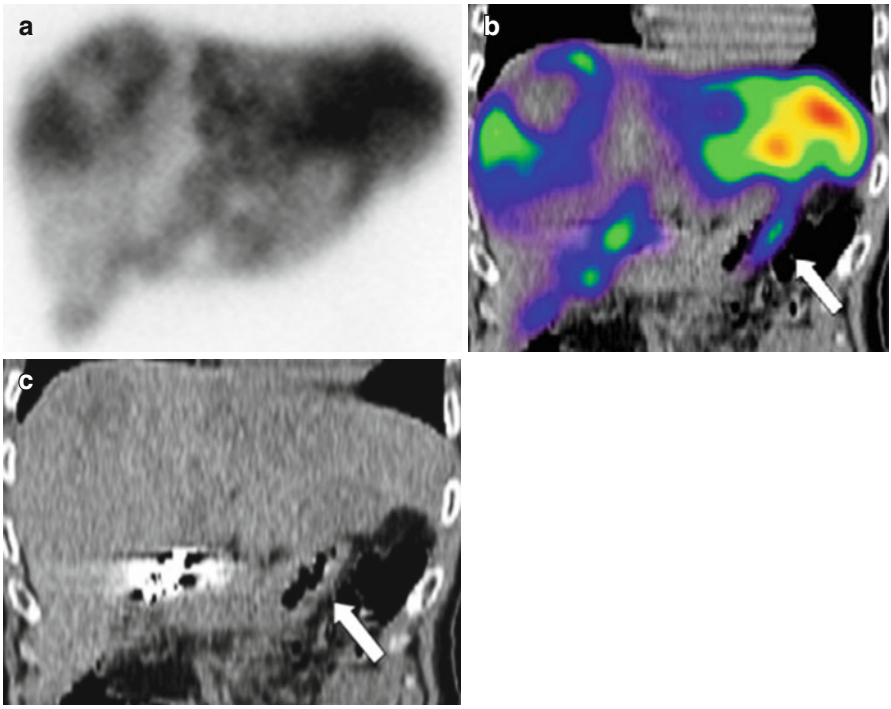

Fig. 2.3 Duodenal accumulation (*arrows*) in a patient with colorectal cancer, not definable on planar images: planar scan (**a**), SPECT/CT coronal view (**b**) and CT coronal view (**c**) (Reprinted from Ahmadzadehfar et al. [32] with permission of the Society of Nuclear Medicine)

background activity ranging from 0 to 1 GBq including two cylindrical active sources independently ranging from 0 to 0.7 GBq. The deviation activity ranged from −9.5 to 4.1 % and from −14.9 to 4.3 %, for the whole phantom and for the sources, respectively. The total body activity deviation on five treated patients versus the injected activity (mean ± std activity = 8.9 ± 0.9 GBq) ranged from −4.9 to 0.0 % with dead-time correction (from −15.2 to −10.2 % without).

Those studies show that SPECT/CT can be used for individualised dosimetry treatment planning. The maximal safe activity found to be injected can be reduce by 10 % in order to account for the current quantification accuracy.

Ahmadzadehfar et al. [32] evaluated the impact of ^{99m}Tc-MAA SPECT/CT on SIRT treatment planning and its added value to angiography in 90 studies performed on 76 patients. The accurate co-registration of the two modalities obtained with a hybrid SPECT/CT system allows determining in a robust way which tissue corresponds to the activity observed (Fig. 2.3). Extrahepatic accumulation was detected by planar imaging, SPECT and SPECT/CT in 12, 17 and 42 % of examinations, respectively. The sensitivity for detecting extrahepatic shunting with planar imaging, SPECT and SPECT/CT was 32, 41 and 100 %, respectively, all with a specificity higher than 93 %. They concluded that

^{99m}Tc-MAA SPECT/CT is valuable for identifying extrahepatic visceral sites at risk for postradioembolisation complications.

2.4 Choice of a Surrogate

^{90}Y is the major used radionuclide in internal radiotherapy which does not own any isotope having an appropriated half-life and emitting γ-rays that can be imaged by SPECT. The choice of the good SPECT surrogate is a crucial point which has not yet been sufficiently investigated. ^{90}Y is mainly used in PRRT, radio-immunotherapy and liver radioembolisation.

When introducing PRRT the community thought that tissues uptake should mainly depend on the peptide, perhaps a little bit on the chelator and marginally on the radionuclide which is confined in the chelator cage. Later, Reubi et al. showed that receptor affinity for a same chelator-peptide also strongly depends on the labelled radionuclide [33], e.g. by a factor 2 when replacing Y by Ga in DOTATATE labelling. However, contrary to tumours, organ uptakes are not always only receptor dependent. For example, an important part of the ^{90}Y-DOTATOC kidney uptake is not receptor dependent and ^{111}In-DOTATOC-based dosimetry has shown a good correlation with kidney toxicity post-therapy [6].

However, this shows that the choice of a radionuclide surrogate for individualised treatment planning in PRRT requires an initial validation proving identical pharmacokinetics along a patient per patient basis. Such studies in PRRT are still lacking. This validation can be performed by imaging the ^{90}Y therapy by bremsstrahlung SPECT or by PET imaging of the compound labelled with ^{86}Y [34], however, both modalities requiring state-of-the-art correction methods.

In radio-immunotherapy, Minarik et al. [35] compared in three patients the absorbed doses obtained from a pre-therapeutic 300 MBq ^{111}In-ibritumomab SPECT/CT to those obtained post-^{90}Y-ibritumomab therapy by bremsstrahlung SPECT/CT using corrections developed on site (see Bremsstrahlung SPECT/CT chapter). The absolute relative differences between absorbed dose computed from ^{111}In and ^{90}Y SPECT/CT were 8.8 ± 13.7 and 8.9 ± 4.0 (mean ± std in %), for the liver and kidneys, respectively. This supports considering ^{111}In as a surrogate of ^{90}Y in radio-immunotherapy. Compared to peptides, the active site in antibodies is located farther from the radionuclide which likely reduces its impact. However, a validation on a larger patient series is still needed.

For ^{90}Y-loaded glass microspheres, Chiesa et al. [24] performed in 35 patients a co-registering of the ^{99m}Tc-MAA SPECT with the ^{90}Y bremsstrahlung SPECT. In the 29 patients treated with the same intentional catheter positioning that in the pre-therapeutic study, the biodistribution was markedly different between the two modalities in two patients (7 %) and seems only attributable to the different physical properties of microspheres and MAA.

For ^{90}Y resin microspheres, Jiang et al. [36] conducted an interesting study in 81 paired ^{99m}Tc-MAA and ^{90}Y bremsstrahlung SPECT performed in 75 patients, the catheter being intended to be set in the same position in the two radioembolisations

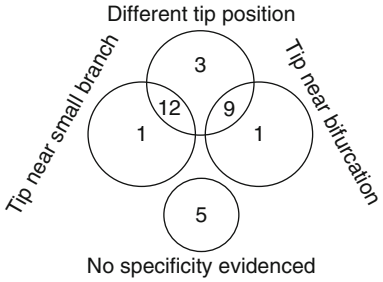

Fig. 2.4 Summary of results from [36] that analysed in the angiograms the catheter tip position in paired studies showing a segmental perfusion difference (SPD) between ^{99m}Tc-MAA and ^{90}Y SPECT, i.e. 31 out of 81 resin microspheres radioembolisations

using angiography. They observed a segmental perfusion difference (SPD) between the two SPECT modalities in 31 patients. Analysing the position of the catheter tip on the two angiograms performed, they noted that 24 SPDs correspond to a different tip position between the two radioembolisations; 2 SPDs occurred with the same tip position but close to an arterial bifurcation or close to a small branch (Fig. 2.4). However, in 5 SPDs no particular specificity was evidenced besides the physical properties of the particles.

These two studies suggest that ^{99m}Tc-MAA is not appropriate for individual dosimetry treatment planning in liver radioembolisation. Regarding also the challenge to identically repeat the two catheterisations, especially when the tip has to be set close to a bifurcation or a small branch, the future could be in tracking the microspheres' deposition during the catheterisation (see Bremsstrahlung SPECT chapter).

2.5 SPECT/CT-Based Dose-Response Studies

Garin et al. [7] performed a dose-response retrospective study in 36 patients for HCC treated with ^{90}Y-loaded glass microspheres. The absorbed doses to liver and tumours were assessed using the ^{99m}Tc-MAA SPECT/CT performed within 1–2 weeks before the therapy and iteratively reconstructed with attenuation and with dual-energy windows scatter correction. The catheter line was counted after therapy in order to estimate the actual injected activity. The planned absorbed dose to the targeted liver volume was 120 Gy based on the MAA, without exceeding 30 Gy for the lungs. Compared to the planning only using the lung shunt and the targeted liver volume, this dose assessment allowed increasing the injected activity in four patients owning large lesions. Mean absorbed doses for nonresponding and responding tumours were 124 ± 63 Gy and 328 ± 107 Gy, respectively. The 30-month overall survival evidenced a 205 Gy tumour-absorbed dose responding threshold (Fig. 2.5).

Chiesa et al. [37, 38] retrospectively analysed treatment with ^{90}Y-loaded glass microspheres in 52 patients (36, 7 and 9 Child–Pugh A5, A6 and B7, respectively). Voxel dosimetry was computed from the ^{99m}Tc-MAA SPECT performed within

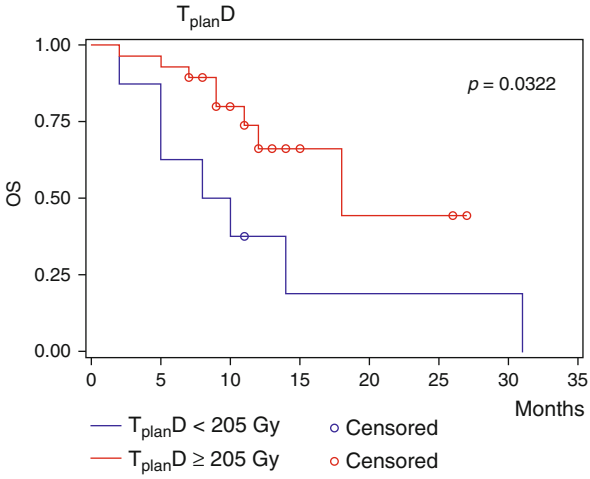

Fig. 2.5 Kaplan–Meier estimates of overall survival (*OS*) stratified by tumour dose (Reprinted from Garin et al. [7] with permission of the Society of Nuclear Medicine)

3–4 weeks before the therapy and corrected for attenuation using CT co-registration. All the administrations were lobar, aiming to deliver a mean absorbed dose of 120 Gy to the target lobe including tumour based on the lobe mass measured on CT. There was an overlap in the absorbed doses of the nonresponding tumours (0 → 500 Gy) and of the responding tumours (250 → 1,500 Gy).

Strigari et al. [8] retrospectively analysed HCC treatment with ^{90}Y-resin microspheres in 73 patients. The administered activity was determined using the BSA method. Entire liver was treated in 35 patients; a right and left lobar approach was used in 35 and 3 patients, respectively. The liver and tumour dosimetry was assessed on the fusion of the pre-therapeutic ^{99m}Tc-MAA SPECT with a CT using a dedicated software. An elliptical constant attenuation map was used in the SPECT reconstruction with an effective attenuation coefficient of 0.11 cm^{-1} to account for the scatter. The TCP fit, based on RECIST or EASL criteria, showed that two different radioresistant tumour populations coexisted: 60 and 40 % of the tumours had a TD_{50} around a BED of 50 and 130 Gy, respectively. Complete response was observed in all tumours above BED = 200 Gy (AD = 145).

This much higher threshold for tumour response observed in liver-radioembolisation studies compared to the traditional 40 Gy observed in EBRT is partly explained by the fact that in internal therapy due to the beta range, the outer shell of the tumour receives about half of the mean absorbed.

2.6 SPECT/CT-Based Dose–Toxicity Studies

In the study [8] summarised here above, Strigari et al. measured a median liver dose of 36 Gy ranging from 6 to 78 Gy. 58, 13 and 2 patients were classified Child–Pugh A, B and C, respectively. The liver was considered as a purely parallel organ ($n = 1$ in the Lyman–Burman Kutcher model). Liver BED was computed with $\alpha/\beta = 2.5$ Gy and using 2.5 h for the sublethal damage repair half-time. The common terminology

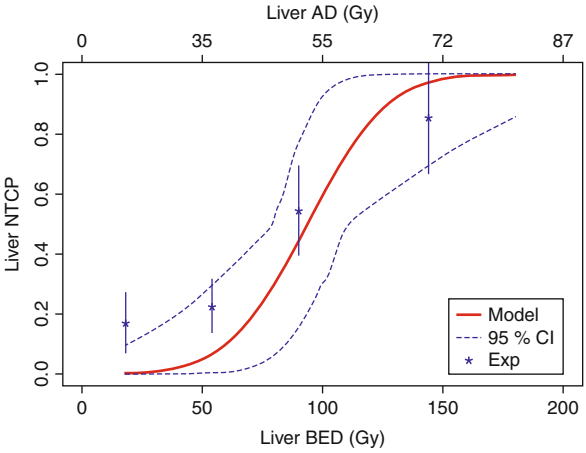

Fig. 2.6 Normal tissue complication probability of liver toxicity (*solid line*) vs. liver BED. *Dashed line* represents 95 % confidence interval. Vertical bars represent SD (caused by number of data in each group that created each point). *Exp* experimental data (Reprinted from Strigari et al. [8] with authorisation of the Society of Nuclear Medicine Liver; absorbed dose (AD) were added by the author of the present chapter)

criteria for adverse events (version 4 National Cancer Institute, Cancer Therapy Evaluation Program) were used to qualify late liver toxicity (4.5 months follow-up). Figure 2.6 shows the liver toxicity–dose relationship considering grades ≥2 as liver toxicity threshold, i.e. at least severe or medically significant.

In the study [37, 38] summarised in the previous section, Chiesa et al. assessed the liver toxicity as the occurrence, during the first 6 months after therapy, of any of the following: clinically detectable ascites, hepatic encephalopathy, bleeding from oesophageal varices, total bilirubin >3 mg/dL and prothrombin time INR (international normalised ratio) >2.2. Figure 2.7a shows that the NCTP strongly depends on the Child–Pugh status. Figure 2.7b shows that for Child–Pugh A, the $NCTP_{50}$ occurred around AD = 100 Gy, twofold higher than the AD = 50 Gy observed by Strigari et al. (Fig. 2.6).

For the time being, this difference in hepatic toxicity cannot be explained only by the much less number of glass microspheres per GBq compared to that of resin microspheres. Gulec et al. [39] performed micro-dosimetry computation by Monte Carlo in a realistic liver model for a mean liver absorbed dose of 64 Gy. As shown in Table 2.1, in therapeutic condition, glass microspheres deliver in all hepatic tissues an absorbed dose significantly higher than that delivered by resin microspheres or by 40 Gy-EBRT. The central vein being the tissue located at the farthest distance to the microspheres, no other hepatic tissue can receive a lower dose. The understanding issues of lower glass microspheres toxicity remain open.

Smits et al. [40] conducted a phase 1 dose-escalation study in ^{166}Ho liver radioembolisation with a state-of-the-art design. Six, 3, 3 and 3 patients received activities in order to get a whole-liver absorbed dose of 20, 40, 60 and 80 Gy, respectively, calculated assuming a homogeneous distribution of the activity in the whole liver, i.e. neglecting the tumour liver burden. After coil embolisation of undesirable artery branch, ^{99m}Tc-MAA were injected and followed by a SPECT or SPECT/CT imaging. Within 2 weeks a second angiography was performed with injection of a 250 MBq scout activity of ^{166}Ho microspheres following by a SPECT or SPECT/CT imaging. The same day a third angiography was performed with injection of the

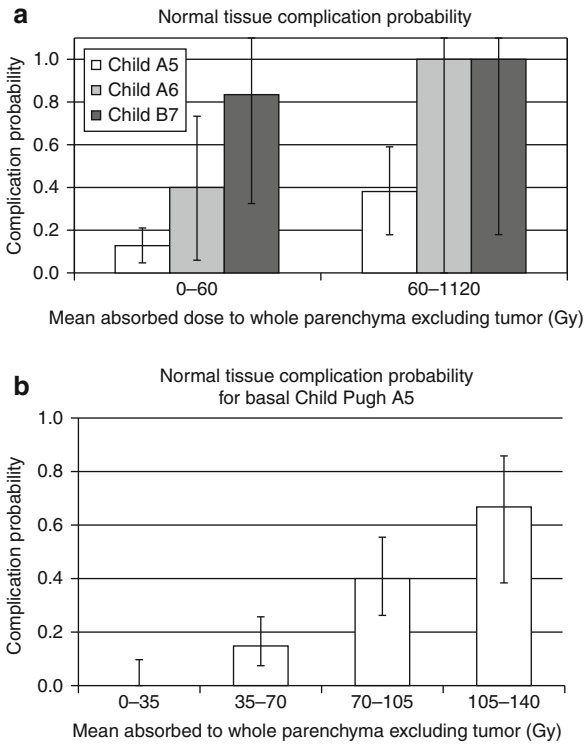

Fig. 2.7 NTCP histogram in function of mean absorbed dose to the lobe excluding tumour for the different Child–Pugh populations (Reprinted from Chiesa et al. [37] with permission of Minerva Medica)

Table 2.1 Microscopic dosimetry in liver obtained from Monte Carlo simulations [39]

	64Gy mean liver dose		Recommended therapy	
	AD (resin) [Gy]	AD (glass) [Gy]	AD (resin) [Gy]	AD (glass) [Gy]
Liver (excluding tumour)	64	64	40	120
Hepatic artery	188	58–339	118	110–645
Bile duct	112	58–171	71	110–326
Portal vein	109	58–167	69	110–318
Central vein	59	58	38	110

therapeutic ^{166}Ho microspheres activity. Both ^{166}Ho radioembolisations intended the same catheter positioning than that in the ^{99m}Tc-MAA one. SPECT or SPECT/CT and MRI imaging were performed 3–5 days post-therapy. In all patients the three SPECT modalities showed similar patterns of the presence or absence of extrahepatic deposition of activity. Regarding the adverse events, the authors concluded that ^{166}Ho radioembolisation with a whole-liver dose of 60 Gy is feasible.

Unfortunately, in addition to the limited patients series, for the time being the authors reported the adverse events and the tumours responses only in function of the aimed absorbed dose. Reporting in function of the actual absorbed doses individually measured by the post-therapy, ^{166}Ho SPECT should scientifically be very valuable. Also, comparing the liver and tumours activity distribution between the three SPECT

modalities with regard to the tip position, as performed by Jiang et al. [36] (see above), should allow to assess independently the impact of the physical properties of the particles and of the part of inevitable variability in catheterisation procedures.

Conclusions

SPECT/CT undoubtedly provided a much better accuracy for individual dosimetry assessment than planar imaging. The reported activity quantification accuracy is better than 10 %, definitely allowing the use of SPECT/CT for individualised treatment planning. This implementation should significantly improve the patient outcome. For some internal radiotherapies, a weakness of SPECT/CT is the need to use a radioisotope surrogate. The choice of this surrogate has to be carefully investigated in order to prove an identical pharmacokinetics on a patient per patient basis.

References

1. Barone R, Borson-Chazot F, Valkema R, Walrand S, Chauvin F, Gogou L, Kvols LK, Krenning EP, Jamar F, Pauwels S. Patient-specific dosimetry in predicting renal toxicity with (90) Y-DOTATOC: relevance of kidney volume and dose rate in finding a dose-effect relationship. J Nucl Med. 2005;46:99S–106.
2. Pauwels S, Barone R, Walrand S, Borson-Chazot F, Valkema R, Kvols LK, Krenning EP, Jamar F. Practical dosimetry of peptide receptor radionuclide therapy with (90)Y-labeled somatostatin analogs. J Nucl Med. 2005;46:92S–8.
3. Walrand S, Lhommel R, Goffette P, Van den Eynde M, Pauwels S, Jamar F. Hemoglobin level significantly impacts the tumor cell survival fraction in humans after internal radiotherapy. EJNMMI Res. 2012;2:20.
4. Walrand S, Barone R, Pauwels S, Jamar F. Experimental facts supporting a red marrow uptake due to radiometal transchelation in 90Y-DOTATOC therapy and relationship to the decrease of platelet counts. Eur J Nucl Med Mol Imaging. 2011;38(7):1270–80.
5. Flamen P, Vanderlinden B, Delatte P, Ghanem G, Ameye L, Van Den Eynde M, Hendlisz A. Multimodality imaging can predict the metabolic response of unresectable colorectal liver metastases to radioembolization therapy with Yttrium-90 labeled resin microspheres. Phys Med Biol. 2008;53(22):6591–603.
6. Wessels BW, Konijnenberg MW, Dale RG, Breitz HB, Cremonesi M, Meredith RF, Green AJ, Bouchet LG, Brill AB, Bolch WE, Sgouros G, Thomas SR. MIRD pamphlet No. 20: the effect of model assumptions on kidney dosimetry and response–implications for radionuclide therapy. J Nucl Med. 2008;49(11):1884–99.
7. Garin E, Lenoir L, Rolland Y, Edeline J, Mesbah H, Laffont S, Porée P, Clément B, Raoul JL, Boucher E. Dosimetry based on 99mTc-macroaggregated albumin SPECT/CT accurately predicts tumor response and survival in hepatocellular carcinoma patients treated with 90Y-loaded glass microspheres: preliminary results. J Nucl Med. 2012;53(2):255–63.
8. Strigari L, Sciuto R, Rea S, Carpanese L, Pizzi G, Soriani A, Iaccarino G, Benassi M, Ettorre GM, Maini CL. Efficacy and toxicity related to treatment of hepatocellular carcinoma with 90Y-SIR spheres: radiobiologic considerations. J Nucl Med. 2010;51(9):1377–85.
9. Jamar F, Barone R, Mathieu I, Walrand S, Labar D, Carlier P, de Camps J, Schran H, Chen T, Smith MC, Bouterfa H, Valkema R, Krenning EP, Kvols LK, Pauwels S. 86Y-DOTA0-D-Phe1–Tyr3-octreotide (SMT487)–a phase 1 clinical study: pharmacokinetics, biodistribution and renal protective effect of different regimens of amino acid co-infusion. Eur J Nucl Med Mol Imaging. 2003;30(4):510–8.

10. Gay HA, Niemierko A. A free program for calculating EUD-based NTCP and TCP in external beam radiotherapy. Phys Med. 2007;23:115–25.
11. Adler JR, Chang SD, Murphy MJ, Doty J, Geis P, Hancock SL. The Cyberknife: a frameless robotic system for radiosurgery. Stereotact Funct Neurosurg. 1997;69:124–8.
12. Devic S. MRI simulation for radiotherapy treatment planning. Med Phys. 2012;39(11):6701–11.
13. Scripes PG, Yaparpalvi R. Technical aspects of positron emission tomography/computed tomography in radiotherapy treatment planning. Semin Nucl Med. 2012;42(5):283–8.
14. Götz L, Spehl TS, Weber WA, Grosu AL. PET and SPECT for radiation treatment planning. Q J Nucl Med Mol Imaging. 2012;56(2):163–72.
15. Taylor ML, Kron T, Franich RD. A contemporary review of stereotactic radiotherapy: inherent dosimetric complexities and the potential for detriment. Acta Oncol. 2011;50(4):483–508.
16. Berker Y, Goedicke A, Kemerink GJ, Aach T, Schweizer B. Activity quantification combining conjugate-view planar scintigraphies and SPECT/CT data for patient-specific 3-D dosimetry in radionuclide therapy. Eur J Nucl Med Mol Imaging. 2011;38(12):2173–85.
17. Sandström M, Garske U, Granberg D, Sundin A, Lundqvist H. Individualized dosimetry in patients undergoing therapy with (177)Lu-DOTA-D-Phe (1)-Tyr (3)-octreotate. Eur J Nucl Med Mol Imaging. 2010;37(2):212–25.
18. Garkavij M, Nickel M, Sjögreen-Gleisner K, Ljungberg M, Ohlsson T, Wingårdh K, Strand SE, Tennvall J. 177Lu-[DOTA0, Tyr3] octreotate therapy in patients with disseminated neuroendocrine tumors: Analysis of dosimetry with impact on future therapeutic strategy. Cancer. 2010;116(4):1084–92.
19. Valkema R, Pauwels S, Kvols LK, Kwekkeboom DJ, Jamar F, de Jong M, et al. Long-term follow-up of renal function after peptide receptor radiation therapy with 90Y-DOTA0, Tyr3-octreotide and 177Lu-DOTA0, Tyr3-octreotate. J Nucl Med. 2005;46:83S–91.
20. Konijnenberg M, Melis M, Valkema R, Krenning E, de Jong M. Radiation dose distribution in human kidneys by octreotides in peptide receptor radionuclide therapy. J Nucl Med. 2007;48(1):134–42.
21. Bouchet LG, Bolch WE, Blanco HP, Wessels BW, Siegel JA, Rajon DA, Clairand I, Sgouros G. MIRD Pamphlet No 19: absorbed fractions and radionuclide S values for six age-dependent multiregion models of the kidney. J Nucl Med. 2003;44(7):1113–47.
22. De Jong M, Valkema R, Van Gameren A, et al. Inhomogeneous localization of radioactivity in the human kidney after injection of [111In-DTPA]octreotide. J Nucl Med. 2004;45:1168–71.
23. Cremonesi M, Ferrari M, Bartolomei M, Orsi F, Bonomo G, Aricò D, Mallia A, De Cicco C, Pedroli G, Paganelli G. Radioembolisation with 90Y-microspheres: dosimetric and radiobiological investigation for multi-cycle treatment. Eur J Nucl Med Mol Imaging. 2008;35(11):2088–96.
24. Chiesa C, Maccauro M, Romito R, Spreafico C, Pellizzari S, Negri A, Sposito C, Morosi C, Civelli E, Lanocita R, Camerini T, Bampo C, Bhoori S, Seregni E, Marchianò A, Mazzaferro V, Bombardieri E. Need, feasibility and convenience of dosimetric treatment planning in liver selective internal radiation therapy with (90)Y microspheres: the experience of the National Tumor Institute of Milan. Q J Nucl Med Mol Imaging. 2011;55(2):168–97.
25. Lhommel R, van Elmbt L, Goffette P, Van den Eynde M, Jamar F, Pauwels S, Walrand S. Feasibility of 90Y TOF PET-based dosimetry in liver metastasis therapy using SIR-Spheres. Eur J Nucl Med Mol Imaging. 2010;37(9):1654–62.
26. Brown S, Bailey DL, Willowson K, Baldock C. Investigation of the relationship between linear attenuation coefficients and CT Hounsfield units using radionuclides for SPECT. Appl Radiat Isot. 2008;66(9):1206–12.
27. Ritt P, Vija H, Hornegger J, Kuwert T. Absolute quantification in SPECT. Eur J Nucl Med Mol Imaging. 2011;38:S69–77.
28. Shcherbinin S, Celler A, Belhocine T, Vanderwerf R, Driedger A. Accuracy of quantitative reconstructions in SPECT/CT imaging. Phys Med Biol. 2008;53:4595–604.
29. Vandervoort E, Celler A, Harrop R. Implementation of an iterative scatter correction, the influence of attenuation map quality and their effect on absolute quantitation in SPECT. Phys Med Biol. 2007;52:1527–45.

30. Willowson K, Bailey DL, Baldock C. Quantitative SPECT reconstruction using CT-derived corrections. Phys Med Biol. 2008;53(12):3099–112.
31. Beauregard JM, Hofman MS, Pereira JM, Eu P, Hicks RJ. Quantitative (177)Lu SPECT (QSPECT) imaging using a commercially available SPECT/CT system. Cancer Imaging. 2011;11:56–66.
32. Ahmadzadehfar H, Sabet A, Biermann K, Muckle M, Brockmann H, Kuhl C, Wilhelm K, Biersack HJ, Ezziddin S. The significance of 99mTc-MAA SPECT/CT liver perfusion imaging in treatment planning for 90Y-microsphere selective internal radiation treatment. Nucl Med. 2010;51(8):1206–12.
33. Reubi JC, Schär JC, Waser B, Wenger S, Heppeler A, Schmitt JS, Mäcke HR. Affinity profiles for human somatostatin receptor subtypes SST1-SST5 of somatostatin radiotracers selected for scintigraphic and radiotherapeutic use. Eur J Nucl Med. 2000;27(3):273–82.
34. Walrand S, Flux GD, Konijnenberg MW, Valkema R, Krenning EP, Lhommel R, Pauwels S, Jamar F. Dosimetry of yttrium-labelled radiopharmaceuticals for internal therapy: 86Y or 90Y imaging? Eur J Nucl Med Mol Imaging. 2011;38:S57–68.
35. Minarik D, Sjögreen-Gleisner K, Linden O, Winga K, Tennvall J, Strand S-E, Ljungberg M. 90Y Bremsstrahlung imaging for absorbed-dose assessment in high-dose radioimmunotherapy. J Nucl Med. 2010;51:1974–8.
36. Jiang M, Fischman A, Nowakowski FS, Heiba S, Zhang Z, Knesaurek K, Weintraub J, Josef Machac J. Segmental perfusion differences on paired Tc-99m macroaggregated albumin (MAA) hepatic perfusion imaging and Yttrium-90 (Y-90) bremsstrahlung imaging studies in SIR-sphere radioembolization: associations with angiography. J Nucl Med Radiat Ther. 2012;3:1.
37. Chiesa C, Mira M, Maccauro M, Romito R, Spreafico C, Sposito C, Bhoori S, Morosi C, Pellizzari S, Negri A, Civelli E, Lanocita R, Camerini T, Bampo C, Carrara M, Seregni E, Marchianò A, Mazzaferro V, Bombardieri E. A dosimetric treatment planning strategy in radioembolization of hepatocarcinoma with 90Y glass microspheres. Q J Nucl Med Mol Imaging. 2012;56(6):503–8.
38. Mazzaferro V, Sposito C, Bhoori S, Romito R, Chiesa C, Morosi C, Maccauro M, Marchianò A, Bongini M, Lanocita R, Civelli E, Bombardieri E, Camerini T, Spreafico C. Yttrium-90 radioembolization for intermediate-advanced hepatocellular carcinoma: a phase 2 study. Hepatology. 2012. doi:10.1002/hep.26014.
39. Gulec SA, Sztejnberg ML, Siegel JA, Jevremovic T, Stabin M. Hepatic structural dosimetry in (90)Y microsphere treatment: a Monte Carlo modeling approach based on lobular microanatomy. J Nucl Med. 2010;51(2):301–10.
40. Smits ML, Nijsen JF, van den Bosch MA, Lam MG, Vente MA, Mali WP, van Het Schip AD, Zonnenberg BA. Holmium-166 radioembolisation in patients with unresectable, chemorefractory liver metastases (HEPAR trial): a phase 1, dose-escalation study. Lancet Oncol. 2012;13(10):1025–34.